Supplementary Information

I. Sample details

In the set of experiments described in the main body, we study an InAs/GaAs QDM in which the QDs are separated by 3 nm of GaAs, 3 nm of $Al_{0.3}Ga_{0.7}As$, and another 3 nm of GaAs, which act as the electron tunneling barrier. The vertically-stacked QDMs are separated by 40-nm-thick intrinsic GaAs from an n-doped (10^{15} cm^{-3} Si) GaAs buffer layer on an n-type GaAs substrate. These QD complexes are capped by a 280-nm-thick intrinsic GaAs, followed by 25 nm of $Al_{0.3}Ga_{0.7}As$ as a current blocker. This entire structure is contained within a Schottky diode, allowing for the deterministic loading of electrons into the QDM, as well as energy level tuning via the DC Stark shift. For this particular QDM, the upper QD (3.2 nm) is made thicker than the lower QD (2.6 nm).

II. Stark shift modulation spectroscopy details

All of the data data displayed in the paper were measure using Stark shift modulated absorption spectroscopy, where the sample is modulated at 10 kHz with a 100 mV peak-to-peak square wave, and the transmitted intensity is measured by an avalanche photodiode (APD) connected to a lock-in amplifier. The dipole moments for transitions ω_{25}, ω_{26}, ω_{47} and ω_{48} are theoretically of equal magnitude and are estimated to be 0.086 ueV/sqrt(nW), or equivalently 15 Debye, assuming a focal spot size of 1 um in GaAs. For all other transitions, the dipole moments are reduced by a factor of sqrt(2).

III. Modeling QDM-field interaction of the eight-level system using master equations

To prepare the system in *T*. state, one simply follows the configuration as shown in Fig. S1a. As mentioned in the main text, this is the case where the resonance seems to follow the scanning of the laser, giving rise to absorption profiles with round tops. (Fig. S1b) When Pump 3 is applied to stabilized the nuclear spins (Fig. S1c), a dark-state spectrum is recovered, as revealed in Fig. S1d. The best-fit value for ground state dephasing time T_2^* in this case is determined to be 90 ns. The shorter T_2^* extracted here compared to the case presented in the main text is mainly due the larger standard deviation around the minimum of the dark-state dip. This is likely a result of inadequate nuclear spin locking arising from a slight deviation of the pump detunings from the two-photon resonance, as evident by the "kink" in the spectrum at the probe detuning of -2.5 μeV. The procedure for fitting the dark-state lineshape using the eight-level master equation is outlined below.

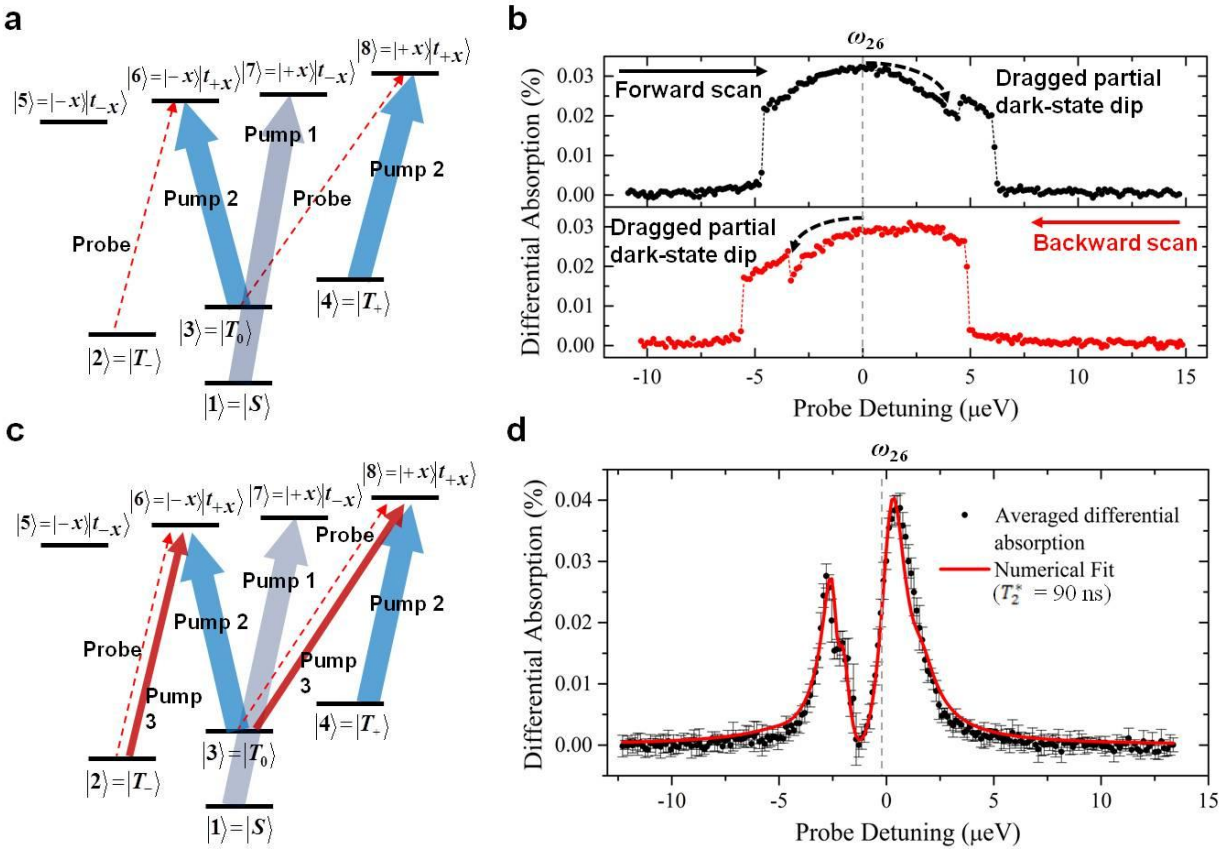

Figure S1 a. Pump configuration for T_- state preparation. **b.** Probe absorption spectra following the pumping scheme in **a.** In the upper panel, the horizontally polarized probe is scanned in forward direction across ω_{26} (= ω_{38}) transition. In the lower panel, the probe laser is scanned in backward direction. **c.** Pump 3 is added to the configuration shown in **a** to suppress the effect of DNSP. **d.** Probe absorption spectrum showing the recovery of dark-state profile. Solid circles in the plot represent averaged data points obtained from a series of 7 scans and the error bars show standard deviations. Red (Grey) solid lines is the theoretical fit.

Using dipole and Rotating-wave approximations, we write the Hamiltonian for the QDM-field system in Schrödinger picture as

$$H_S = \hbar \begin{bmatrix} \nu_1 & 0 & 0 & 0 & 0 & 0 & -\frac{\tilde{\chi}_1(t)}{\sqrt{2}} & 0 \\ 0 & \nu_2 & 0 & 0 & 0 & \tilde{\chi}_3(t)+\tilde{\chi}_p(t) & 0 & 0 \\ 0 & 0 & \nu_3 & 0 & 0 & \frac{\tilde{\chi}_2(t)}{\sqrt{2}} & 0 & \frac{\tilde{\chi}_3(t)+\tilde{\chi}_p(t)}{\sqrt{2}} \\ 0 & 0 & 0 & \nu_4 & 0 & 0 & 0 & \tilde{\chi}_2(t) \\ 0 & 0 & 0 & 0 & \nu_5 & 0 & 0 & 0 \\ 0 & \tilde{\chi}_3^*(t)+\tilde{\chi}_p^*(t) & \frac{\tilde{\chi}_2^*(t)}{\sqrt{2}} & 0 & 0 & \nu_6 & 0 & 0 \\ -\frac{\tilde{\chi}_1^*(t)}{\sqrt{2}} & 0 & 0 & 0 & 0 & 0 & \nu_7 & 0 \\ 0 & 0 & \frac{\tilde{\chi}_3^*(t)+\tilde{\chi}_p^*(t)}{\sqrt{2}} & \tilde{\chi}_2^*(t) & 0 & 0 & 0 & \nu_8 \end{bmatrix} \quad (1)$$

The matrix elements are defined as

$$\nu_1 = -J_{ex} \qquad \nu_5 = \omega_0 - \frac{\mu_B}{2\hbar}(g_e - 3g_h)B$$

$$\nu_2 = -\frac{\mu_B}{\hbar} g_e B \qquad \nu_6 = \omega_0 - \frac{\mu_B}{2\hbar}(g_e + 3g_h)B$$

$$\nu_3 = 0 \qquad \nu_7 = \omega_0 + \frac{\mu_B}{2\hbar}(g_e + 3g_h)B$$

$$\nu_4 = \frac{\mu_B}{\hbar} g_e B \qquad \nu_8 = \omega_0 + \frac{\mu_B}{2\hbar}(g_e - 3g_h)B$$

$$\tilde{\chi}_1(t) = \frac{\Omega_1}{2} e^{i\omega_1 t} \qquad \tilde{\chi}_3(t) = \frac{\Omega_3}{2} e^{i\omega_3 t}$$

$$\tilde{\chi}_2(t) = \frac{\Omega_2}{2} e^{i\omega_2 t} \qquad \tilde{\chi}_p(t) = \frac{\Omega_p}{2} e^{i\omega_p t}$$

Here we assume that the energy separation between any two states is much larger than the natural linewidths of the optical transitions, so that each field drives only one transition except where a degeneracy occurs, *e.g.* $\omega_{26} = \omega_{38}$. J_{ex} is the Coulomb-exchange coupling which gives rise to the energy splitting between S and T_0 states. μ_B is the Bohr magneton, B the applied magnetic field, while g_e and g_h are electron and heavy-hole g-factors respectively. ω_0 represents the optical resonance frequency for the triplet transitions at zero magnetic field. The Rabi frequencies for the optical fields are denoted by Ω_1, Ω_2, Ω_3 and Ω_p for Pump 1, Pump 2, Pump 3 and probe respectively and their optical frequencies by ω_1, ω_2, ω_3 and ω_p.

The presence of two fields, Pump 3 and the probe, driving the same transitions makes the computation of steady-state solutions nontrivial. Here, the first-order probe absorption is determined perturbatively from a steady state solution in which all orders in the pump intensities are included, following the approach outlined in Berman & Malinovsky[1]. For convenience in numerical calculations, it is desirable to re-write Eq. (1) in another basis where the exponents in the off-diagonal matrix elements vanish, except for the cases where both Pump 3 and the probe are involved. This can be easily achieved by using the diagonal unitary operator $U(t)$, with its diagonal elements given by $\{e^{-i\omega_1 t/2}, e^{i(\omega_2-\omega_3)t}, 1, e^{i(\omega_3-\omega_2)t}, 1, e^{i\omega_2 t}, e^{i\omega_1 t/2}, e^{i\omega_3 t}\}$. The rotated Hamiltonian, H_f, is then given by

$$H_f = i\hbar\left[\frac{d}{dt}U(t)\right]U^\dagger(t) + U(t)H_S U^\dagger(t)$$

$$= \hbar\begin{bmatrix}
\nu_1 + \frac{\omega_1}{2} & 0 & 0 & 0 & 0 & 0 & \frac{\Omega_1}{2\sqrt{2}} & 0 \\
0 & \nu_2 - \omega_2 + \omega_3 & 0 & 0 & 0 & \frac{\Omega_3 + \Omega_p e^{-i\Delta t}}{2} & 0 & 0 \\
0 & 0 & \nu_3 & 0 & 0 & \frac{\Omega_2}{2\sqrt{2}} & 0 & \frac{\Omega_3 + \Omega_p e^{-i\Delta t}}{2\sqrt{2}} \\
0 & 0 & 0 & \nu_4 + \omega_2 - \omega_3 & 0 & 0 & 0 & \frac{\Omega_2}{2} \\
0 & 0 & 0 & 0 & \nu_5 & 0 & 0 & 0 \\
0 & \frac{\Omega_3^* + \Omega_p^* e^{i\Delta t}}{2} & \frac{\Omega_2^*}{2\sqrt{2}} & 0 & 0 & \nu_6 - \omega_2 & 0 & 0 \\
\frac{\Omega_1^*}{2\sqrt{2}} & 0 & 0 & 0 & 0 & 0 & \nu_7 - \frac{\omega_1}{2} & 0 \\
0 & 0 & \frac{\Omega_3^* + \Omega_p^* e^{i\Delta t}}{2\sqrt{2}} & \frac{\Omega_2^*}{2} & 0 & 0 & 0 & \nu_8 - \omega_3
\end{bmatrix}$$

where $\Delta = \omega_3 - \omega_p$. Let ρ be the 8-by-8 density matrix and its elements denoted by ρ_{ij}. The master equation is

$$\frac{d}{dt}\rho = -\frac{i}{\hbar}\left[H_f, \rho\right] + \text{relaxation} \tag{2}$$

To determine the elements of the relaxation term, we assume that ground state population relaxation is negligible so that the only experimental parameters in the relaxation term are the trion recombination rate, Γ_r and the optical ground state decoherence rate, Γ_g, with $\Gamma_r \gg \Gamma_g$. We further assume a "lumped model" for the ground state decoherence where Γ_g between any two states has the same magnitude. The relaxation term can thus be written explicit as

$$\begin{bmatrix}
\frac{\Gamma_r(\rho_{55}+\rho_{66}+\rho_{77}+\rho_{88})}{4} & -\Gamma_g\rho_{12} & -\Gamma_g\rho_{13} & -\Gamma_g\rho_{14} & -\frac{\Gamma_r\rho_{15}}{2} & -\frac{\Gamma_r\rho_{16}}{2} & -\frac{\Gamma_r\rho_{17}}{2} & -\frac{\Gamma_r\rho_{18}}{2} \\
-\Gamma_g\rho_{21} & \frac{\Gamma_r(\rho_{55}+\rho_{66})}{2} & -\Gamma_g\rho_{23} & -\Gamma_g\rho_{24} & -\frac{\Gamma_r\rho_{25}}{2} & -\frac{\Gamma_r\rho_{26}}{2} & -\frac{\Gamma_r\rho_{27}}{2} & -\frac{\Gamma_r\rho_{28}}{2} \\
-\Gamma_g\rho_{31} & -\Gamma_g\rho_{32} & \frac{\Gamma_r(\rho_{55}+\rho_{66}+\rho_{77}+\rho_{88})}{4} & -\Gamma_g\rho_{34} & -\frac{\Gamma_r\rho_{35}}{2} & -\frac{\Gamma_r\rho_{36}}{2} & -\frac{\Gamma_r\rho_{37}}{2} & -\frac{\Gamma_r\rho_{38}}{2} \\
-\Gamma_g\rho_{41} & -\Gamma_g\rho_{42} & -\Gamma_g\rho_{43} & \frac{\Gamma_r(\rho_{77}+\rho_{88})}{2} & -\frac{\Gamma_r\rho_{45}}{2} & -\frac{\Gamma_r\rho_{46}}{2} & -\frac{\Gamma_r\rho_{47}}{2} & -\frac{\Gamma_r\rho_{48}}{2} \\
-\frac{\Gamma_r\rho_{51}}{2} & -\frac{\Gamma_r\rho_{52}}{2} & -\frac{\Gamma_r\rho_{53}}{2} & -\frac{\Gamma_r\rho_{54}}{2} & -\Gamma_r\rho_{55} & -\Gamma_r\rho_{56} & -\Gamma_r\rho_{57} & -\Gamma_r\rho_{58} \\
-\frac{\Gamma_r\rho_{61}}{2} & -\frac{\Gamma_r\rho_{62}}{2} & -\frac{\Gamma_r\rho_{63}}{2} & -\frac{\Gamma_r\rho_{64}}{2} & -\Gamma_r\rho_{65} & -\Gamma_r\rho_{66} & -\Gamma_r\rho_{67} & -\Gamma_r\rho_{68} \\
-\frac{\Gamma_r\rho_{71}}{2} & -\frac{\Gamma_r\rho_{72}}{2} & -\frac{\Gamma_r\rho_{73}}{2} & -\frac{\Gamma_r\rho_{74}}{2} & -\Gamma_r\rho_{75} & -\Gamma_r\rho_{76} & -\Gamma_r\rho_{77} & -\Gamma_r\rho_{78} \\
-\frac{\Gamma_r\rho_{81}}{2} & -\frac{\Gamma_r\rho_{82}}{2} & -\frac{\Gamma_r\rho_{83}}{2} & -\frac{\Gamma_r\rho_{84}}{2} & -\Gamma_r\rho_{85} & -\Gamma_r\rho_{86} & -\Gamma_r\rho_{87} & -\Gamma_r\rho_{88}
\end{bmatrix}$$

An approximate steady-state solution would have the form

$$\rho_{ij} = \rho_{ij}^{(0)} + \rho_{ij}^{(1)} \tag{3}$$

where $\rho_{ij}^{(0)}$ is the steady-state solution of Eq. (2) with Ω_p equals zero. We take

$$\rho_{ij}^{(1)} = a_{ij} + b_{ij}e^{i\Delta t} + c_{ij}e^{-i\Delta t} \tag{4}$$

as an ansatz and substitute Eq. (3) and (4) into Eq. (2). By equating the constants and coefficients of $e^{\pm i\Delta t}$ terms on both sides of Eq. 2, we obtain a system of linear equations in a_{ij}, b_{ij} and c_{ij}, which are then solved numerically. The sum of the imaginary parts of c_{26} and c_{38} is proportional to the probe absorption. To see this, one simply goes back to Schrödinger picture to find that c_{26} and c_{38} are the coefficients of $e^{i\omega_p t}$ term.

As mentioned in the Method Section, lineshape fitting is accomplished by repeatedly calculating the absorption spectra using different values for the fitting parameters. Fig. S2 below shows the error-squares of the resulting fit when Γ_r and Γ_g are varied. In Fig. S2a, corresponding to the fit of the T_- transition shown in Fig. S1d, an enclosed region of least error-squares is found. Here the best fitting values for Γ_r and Γ_g can be uniquely determined. However, in Fig. S2b for the T_+ transition presented in the main text, there is no such enclave for Γ_g. Nonetheless, a lower bound for the spin coherence time is found to be 1.3 μs. Tables S1 and S2 summarize the physical parameters of the QDM used in this study and the best-fitting parameter values for both cases.

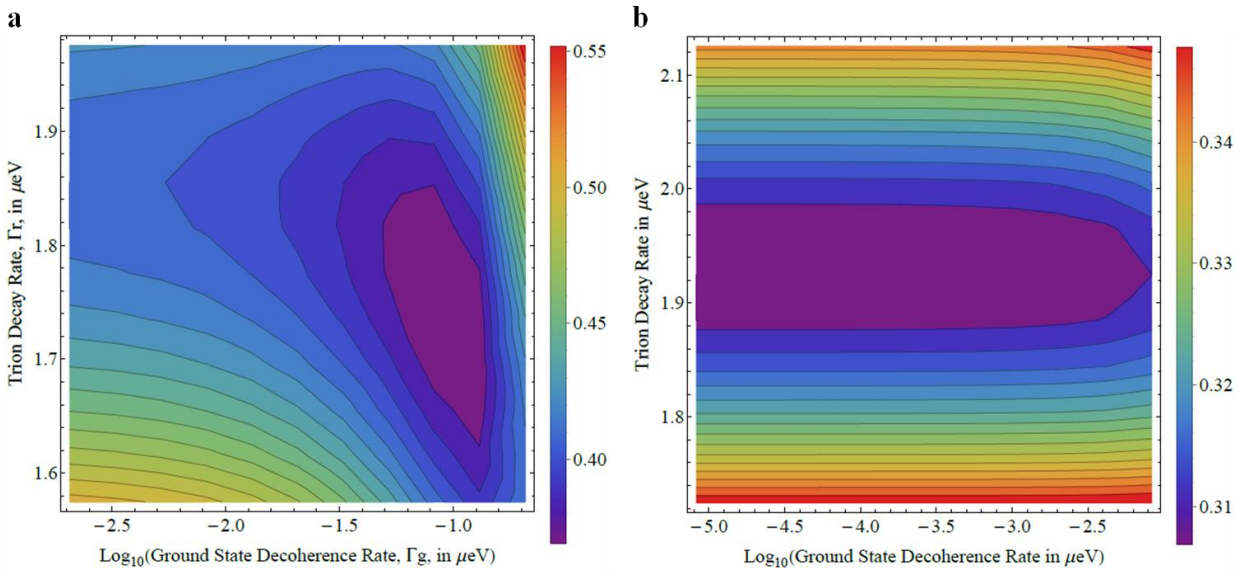

Figure S2: a, Contour plot showing error-squares from the T_- transition lineshape fits calculated by varying the values of Γ_r and Γ_g. The model is based on the pumping scheme shown in Fig. S1c. **b,** Contour plot of the error-squares for calculated T_+ transition lineshapes simulating the pumping scheme in Fig. 2c in the main text.

Table S1: Physical parameters of the QDM used in this study.

Constants	J_{ex}	ω_0	g_e	g_h
Values	116.6	1294.543	0.43	−0.084
Units	μeV	meV	-	-

Table S2: Parameters used to produce the fitting curves. All values are in units of μeV.

Parameters	Ω_1	δ_1^*	Ω_2	δ_2	Ω_3	δ_3	Ω_p	Γ_r	Γ_g
T_- **(Fig. 4b)**	1.96	N/A	1.82	−0.61	0.35	−1.55	0.19	1.78	0.050
T_+ **(Fig. 4d)**	1.86	N/A	1.86	−1.06	0.36	−1.41	0.19	1.93	0.0032

*δ_i denotes detuning from corresponding transition.

III. Estimating the intrinsic nuclear Overhauser field distribution in an InAs QD

An order-of-magnitude estimate of the intrinsic nuclear Overhauser field distribution can be derived as follows: The field contributed by type-α isotope in a single primitive unit cell at position $\boldsymbol{r}$, is given by $\delta B_{\alpha,\boldsymbol{r}} = \frac{a_0^3}{4g_e\mu_B}|\Psi_e(\boldsymbol{r})|^2 A_{\alpha,\boldsymbol{r}}^{en}\hat{I}_{\alpha,\boldsymbol{r}}$, where a_0 is the lattice constant, $\Psi_e(\boldsymbol{r})$ the

electron envelop wavefunction, A_α^{en} the electron-nuclear hyperfine constant and $\hat{I}_{\alpha,\boldsymbol{r}}$ the nuclear spin-projection. The total Overhauser field, B_{OH}, as seen by an electron confined within a QD follows the multinomial distribution which approaches the Gaussian distribution for a large number of nuclei. At the experiment temperature of 6 K, $k_{\mathrm{B}}T$ = 517 μeV, and is much larger than the nuclear-Zeeman splitting[2]. Hence $\bar{I}_\alpha \approx 0$ and the distribution of B_{OH} is given by:

$$f(B_{OH}) = \frac{1}{\sqrt{2\pi}\sigma} e^{-\frac{B_{OH}^2}{2\sigma^2}}, \text{ where}$$

$$\begin{aligned} \sigma &= \sqrt{\textstyle\sum_{\boldsymbol{r},\boldsymbol{\alpha}} \delta B_{\alpha,\boldsymbol{r}}^2} \\ &= \frac{a_0^3}{4 g_e \mu_B} \sqrt{\textstyle\sum_{\boldsymbol{r},\boldsymbol{\alpha}} |\Psi_{\mathrm{e}}(\boldsymbol{r})|^4 \left(A_{\alpha,\boldsymbol{r}}^{en}\right)^2 \hat{I}_{\alpha,\boldsymbol{r}}^2} \\ &\approx \frac{1}{g_e \mu_B} \sqrt{\frac{1}{N} \textstyle\sum_{\boldsymbol{\alpha}} (A_\alpha^{en})^2 \bar{I}_\alpha^2} = \frac{1}{g_e \mu_B} \sqrt{\frac{1}{3N} \textstyle\sum_{\boldsymbol{\alpha}} (A_\alpha^{en})^2 I_\alpha (I_\alpha + 1)} \end{aligned}$$

Here N is the number of unit cells in a single QD and $\bar{I}_\alpha^2$ denotes the average of I_α^2. To arrive at the last expression, we assume a uniform $|\Psi_{\mathrm{e}}(\boldsymbol{r})|^2 = 4/Na_0^3$, and take into account that each *primitive* unit cell contains an In nucleus and an As nucleus. Assuming a cylindrical QD with a diameter of 10 nm and a height of 3 nm, $N \approx 4250$ for a_0 = 6.05 Å. Using A_{In}^{en} = 56 μeV and A_{As}^{en} = 47 μeV for spin-$\frac{9}{2}$ In and spin-$\frac{3}{2}$ As nuclei, respectively[3], we obtain $\sigma \approx 0.11$ Tesla for the standard deviation of the intrinsic B_{OH} distribution. This order-of-magnitude estimate is in agreement with the experimentally determined value of 0.15 Tesla.

IV. Fitting the lineshapes involving finite Overhauser field distributions at singlet transitions of ω_{15} and ω_{18}

As mentioned in the main text and in the Methods section, the numerical fits for Fig. 3b are generated from absorption spectra corresponding to different Overhauser fields. Here, the Rabi frequencies of the pump lasers can be estimated based on the incident powers and the best-fit parameters obtained in Section I. Besides, the detunings can be easily determined from the positions of the dark-state dips. Assuming that Γ_r remains the same, the only fitting parameters need to be considered here are Γ_g and the Overhauser field distribution. The distribution is constructed from three Gaussian curves with different widths, heights and offsets. The same procedure discussed in Section I is used to find the best-fit value for Γ_g and the Overhauser field distribution. Only this time either Γ_g or the Overhauser field distribution is varied in each iteration, and the lineshape is the distribution-weighted average of many spectra calculated from distinct magnetic fields. A graphical example showing the best-fit lineshape corresponding to the intrinsic Overhauser field distribution (without Pump 3, Fig. 3b) and its several constituent spectra are given in Fig. S3 below.

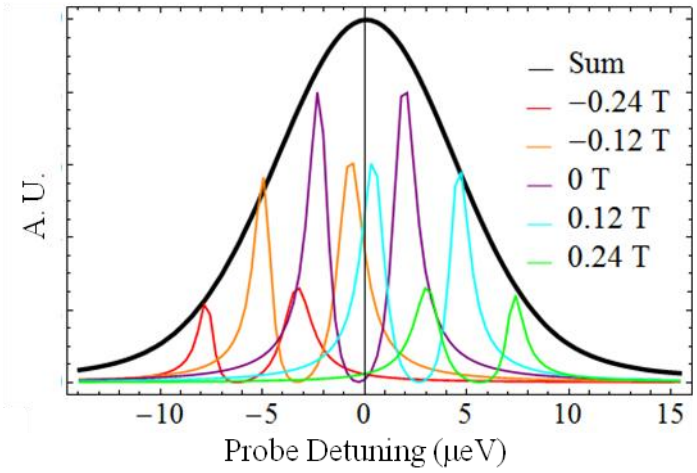

Figure S3: (coloured) Examples of calculated spectra corresponding to a number of selected Overhauser fields and (black) final lineshapes for the "intrinsic" case similar to the one represented by the red solid line shown in Fig. 3b.

References

[1] Berman, P. R., & Malinovsky, V. S. *Principles of Laser Spectroscopy and Quantum Optics*, Princeton University Press, Princeton, New Jersey (2011).

[2] Stone, N.J. Table of nuclear magnetic dipole and electric quadrupole moments. *At. Data Nucl. Data Tables* **90**, 75-176 (2005).

[3] Petrov, M.Y. *et al.* Effect of thermal annealing on the hyperfine interaction in InAs/GaAs quantum dots. *Phys. Rev. B* **78**, 045315 (2008).